

Geometrical constraints in a gene network model and pattern formation

L. Diambra* and Luciano da Fontoura Costa†

Institute of Physics at São Carlos, University of São Paulo.

Caixa Postal 369, cep 13560-970, São Carlos, SP, Brazil.

Phone +55 16 3373 9858, FAX +55 16 3373 9879

Abstract

A fundamental task in developmental biology is to identify the mechanisms which drive morphogenesis. In many cases, pattern formation is driven by the positional information determined by both the gradient of maternal factors and hard-wired mechanisms embedded in the genome. Alternative mechanisms of positional information that contribute to patterning are the influence of signals derived from surrounding tissues. In this paper, we show that the interplay of geometrical constraints imposed by tissue shapes and hard-wired mechanisms, computationally implemented by a gene network model, can be able to induce stable complex patterns. The rise of these patterns depends strongly on the geometrical constraints such as the shape of the surrounding tissues.

PACS numbers: 87.18.Hf, 87.18.La, 87.16.-b, 87.16.Ac, 87.16.Yc

* Electronic address: diambra@if.sc.usp.br (corresponding author)

† Electronic address: luciano@if.sc.usp.br

I. INTRODUCTION

Developmental biology has identified several organizing principles that contribute in an orchestrated manner to embryogenesis and organogenesis. Several cell communication processes, such as lateral inhibition [1], embryonic induction [2], cell growth and death [3] and cell migration [4]; guide the development of tissues and organs. Such the processes are controlled by the information contained in the genome, which is usually the same in all cells. Therefore, a question arises: how do complex patterns emerge from initially homogeneous conditions? One way to address this issue is by morphogenic gradients. Morphogens are signaling molecules that can induce several distinct cell fates in a concentration-dependent manner [5, 6]. The diffusion of a morphogen from a localized source generates a graded distribution across a field of cells. The local concentration of this molecule would induce the fate of nearby cells in a position-dependent manner. Typically, a morphogen is produced by a distinct localized set of cells, from which it moves into surrounding tissues. If certain conditions are met, a spatial gradient of morphogen concentration, decaying away from the source, will result. When a signal is bound to its receptor, a specific intracellular signal transduction pathway is triggered, leading to transcriptional and/or pos-transcriptional changes in responsive cells. If cells can sense the local concentration accurately, then spatial patterns of cell response can be generated. For example, in *Xenopus* embryos, it has been established that bone morphogenetic protein controls neural and epidermal fates in the vertebrate ectoderm, under the control of antagonists secreted by the organizer region of the mesoderm [7]. Also wingless, hedgehog, and decapentaplegic proteins in the *Drosophila* wing imaginal discs, are well studied examples of secreted signaling proteins [8].

From a mathematical point of view, Alan Turing showed a pathway to pattern formation without pre-patterns for its initiation [9, 10]. This self-organized mechanism can be thought of as a competition between activation by a slow diffusing chemical and inhibition by a faster chemical, and has been largely applied to explain biological pattern formation (for example see [9, 11]). However, it is important to keep in mind that biological strategies of patterning can be very different from the self-organized Turing-type mechanisms. Segmentation in *Drosophila* [12, 13] and somitogenesis [14, 15] in vertebrate seem to follow a hard-wired strategy hierarchically organized from small regulatory gene networks. The extent to which patterns under development are self-organized or hard-wired remains an issue of debate

[16, 17, 18].

In this paper we will explore, by means of computational simulations, the role of chemical signaling derived from surrounding tissues to patterning processes. In particular, we will show that specific geometrical constraints, like the shape of morphogen sources, are able to generate nontrivial endogenous gradients which will play a key role in the formation of complex structures. Modeling pattern formation is a current research topic in developmental biology [9, 11, 19, 20, 21] and to the best of our knowledge, the interplay of geometrical constraints, imposed by the shapes of surrounding tissues, and feedback control implemented in a gene network model has never been addressed before. Some studies about the effects of curvature and other geometrical constraint on pattern formation have been described in [22, 23].

In most cases, the shape of endogenous morphogen gradients is rarely known because the absolute concentration of the factor under analysis is so low. Furthermore, the regulatory gene networks, as well as the signalling pathway involved in developmental programs are not, in most cases, quantitatively characterized. For these reasons, in order to illustrate and to test the feasibility of our approach, we use a mathematical model and computational analysis. Our mathematical model sticks to the hard-wired strategy, implementing several negative feedback loops in a generic regulatory gene network. This gene network embedded in endogenous gradients is able to induce stable complex patterns. The rise of these patterns depends strongly on the geometrical constraints such as the shape of the surrounding tissues.

Successful development can take place in a range of environments. Developmental mechanism of patterning must be robust and precise. Signals produced at wrong place or time can lead to an inappropriate developmental process. The relevance of noise and robustness will be also discussed.

II. METHODS

A. Shaping morphogen gradients

Although pattern formation is indeed induced by graded activation of a signaling pathway, several factors are involved in the distribution of a morphogen in a developmental field [24]. The mechanisms involved in gradient shaping is one of the main issues debated in

developmental biology today. Such mechanisms include passive diffusion in the extracellular matrix [25], repeated rounds of endocytosis and exocytosis [26], cytonemes [27], argosomes [28], and a recently proposed mechanism by mRNA decay in growing structures [29]. It is beyond the scope of this paper modeling the shape gradient genesis. We will adopt the simple localized source-dispersed sink models, where the shape of a morphogen gradient is dictated by the rate of diffusion away from the site of synthesis, along with the rate degradation. The gradient can be broadened by either increasing the diffusion rate or decreasing the degradation rate, while the opposite effects can produce a much steeper gradient. In particular, the diffusive substances are secreted by the fixed boundary of surrounding tissues. Thus, we also consider that these substances are degraded over all developmental field. We can represent these processes by the following equations

$$\begin{aligned}\dot{a} &= D_a \nabla^2 a - \lambda_a a \\ \dot{h} &= D_h \nabla^2 h - \lambda_h h,\end{aligned}\tag{1}$$

where a (h) denotes the activator (inhibitor) concentration which is released by the tissue I (tissue II) and degraded over the domain at rate λ_a (λ_h). Fig. 1 shows a schematic representation of surrounding tissues, boundaries (bottom panel) and the concentration profiles a and h over a horizontal segment in the middle of a semi-elliptic domain (top panel).

In order to evidence the key role of geometrical constraints in the patterning process, the overall processes were implemented on both semi-elliptical and semicircular domains. Fig. 2 depicts the concentration fields of activators (A) and inhibitors (B) in a portion of the semi-elliptical domain. For the semicircular domain the concentration fields of activators and inhibitors are shown in (A) and (B) respectively and they were obtained using the parameters in Table 1. Despite of small differences between the top and bottom morphogen distributions, they are sufficient to induce completely different patterns of expression of regulated genes, as we will show later.

B. Hard-wired model for development

The striped pattern of pair-rule genes in *Drosophila* is a consequence of the fact that each stripe is separately controlled by dedicated transcription regulation [12]. This is an

example where biological strategies of patterning seem to follow a hierarchically organized building strategy from small modular regulatory gene networks. We will construct a small regulatory network (see Fig. 3) which is able to produce complex patterns from an initially homogeneous distribution of the genes products. Our mathematical model considers several biochemical and biophysical processes currently present in many biological descriptions, including: diffusion, degradation, noise and of course, regulatory activation and/or repression of gene expressions. The last one forms two negative feedback loops, which seem to be essential control mechanisms in developmental networks [18]. We will describe regulatory activation sigmoidal functions $s^+(x, \theta, n) = x^n / (x^n + \theta^n)$. If the concentration of activator factor is below the threshold θ , the gene is poorly expressed, whereas above this threshold its expression grow until saturate. The regulatory inhibition will be represented by $s^- = \theta^n / (x^n + \theta^n) \equiv 1 - s^+$. Sigmoidal functions, in particular Hill functions, have been used in a variety of genetic regulatory models [20, 21, 30, 31]. In general, there are several regulatory interactions acting over a single gene, and in these cases the resulting expression rates will be described by the product of sigmoidal functions corresponding to each interaction [32], rather than to the additive formulation used in [20, 21, 30]. For the sake of simplicity, our model does not consider other factors as growth, cell division, post-transcriptional regulation, etc., and does not explicitly distinguish between genes and their products.

We will consider five genes which form a small network of interacting genes. Their product concentrations, represented by u_i with $i = 1, \dots, 5$, evolve following the reaction-diffusion equations

$$\dot{u}_i = d_i \nabla^2 u_i + f_i(a, h, \{u_i\}) - \lambda_{u_i} u_i + \eta \epsilon(t) u_i, \quad (2)$$

where f_i represents the regulatory transcription control of gene i , and λ_i is the degradation rate. The last term represents a multiplicative noise. ϵ is a random variable that is assumed uncorrelated and Gaussian distributed (null mean and variance unitary). η represents the intensity of noise. Eq. (2) governs the spatio-temporal evolution of the small regulatory gene network represented in Fig. 3. This network suffers the influence of the surrounding tissues through the biochemical agents concentration of a and h (which are constant at a time). The particular form of f_i depends on the regulatory inputs acting over gene i , and will be discussed later.

In the hierarchically organized hard-wired strategy, the regulatory role of the genes be-

longing to a network could be organized in different levels, for example: positional level, regulatory level, output level, etc.. These levels interact between them to constitute a specific network structure. In this framework, we can understand a complete developmental program as a network of interacting gene networks.

In this spirit, the positional level will be assigned to U1, the gene associated to concentration u_1 . U1 will decode the positional information derived from the geometrical constraints (boundaries) through a and h concentrations. The transcription of gene U1 will be activated when a reaches a threshold θ_{1a} and will be inhibited by h and its own product at the thresholds θ_{1h} and θ_{11} respectively (the top panel of Fig. 1 shows the values of these parameters). Therefore, the expression of u_1 is governed by Eq. 3:

$$f_1(a, h, u_1) = r_1 s^+(a, \theta_{1a}, n_{1a}) s^-(h, \theta_{1h}, n_{1h}) \times s^-(u_1, \theta_{11}, n_{11}). \quad (3)$$

The expression of U1 activates in a concentration-dependent manner the genes U2, U3, and U4, (associated to the concentrations u_2 , u_3 and u_4 respectively), which constitutes essentially a regulatory level of the hierarchy. U2, U3, and U4 are activated at thresholds $\theta_{21} > \theta_{31} > \theta_{41}$, respectively, and each product inhibits the transcription of the other genes, thus forming two negative feedback loops. So, we can write:

$$f_2(\{u_i\}) = r_{22} s^+(u_2, \theta_{22}, n_{22}) + r_{21} s^+(u_1, \theta_{21}, n_{21}) \times s^-(u_3, \theta_{23}, n_{23}) s^-(u_4, \theta_{24}, n_{24}), \quad (4)$$

where $\{u_i\}$ represents the set of variables $\{u_1, u_2, u_3, u_4, u_5\}$. for $r_{22} > 0$ this gene is also self activated. We have added a self activated term in (4) to study their effects over noise control.

$$f_3(\{u_i\}) = r_3 s^+(u_1, \theta_{31}, n_{31}) s^-(u_2, \theta_{32}, n_{32}) \times s^-(u_4, \theta_{34}, n_{34}), \quad (5)$$

$$f_4(\{u_i\}) = r_4 s^+(u_1, \theta_{41}, n_{41}) s^-(u_2, \theta_{42}, n_{42}) \times s^-(u_3, \theta_{43}, n_{43}). \quad (6)$$

Thus the gradient associated to u_1 generates discrete spatial domains of regulatory factors which interact between them and generate a more complicated spatial domain of transcription of the third level of the hierarchy, the output level. For simplicity, we consider also

that this level is constituted by only one gene. Its activation is promoted by u_1 and it is down-regulated by the gene products of the former level, u_2 , u_3 and u_4 .

$$f_5(\{u_i\}) = r_5 s^+(u_1, \theta_{51}, n_{51}) s^-(u_2, \theta_{52}, n_{52}) \times s^-(u_3, \theta_{53}, n_{53}) s^-(u_4, \theta_{54}, n_{54}). \quad (7)$$

The positive and negative feedback loops of the model are shown in Fig. 3. It is important to keep in mind that the model was constructed to illustrate that gene networks, embedded in feedback control principles, can induce or not complex patterns depending on geometrical constraints of the problem. For the aim of our study, this small network is enough. Of course, other kinds of network can be designed to model specific developmental systems.

III. RESULTS

A. Geometrical constraints and gene regulatory network

The boundary problem is completely specified by Eqs. (1), the initial condition (IC) and the boundary condition (BC). In this sense, $a = 1$ over C and null over C' , the two vertical boundary segments are connected by a periodical boundary condition, while the inhibitor is $h = 1$ over C' and null over C , the two vertical boundary segments are connected by periodic boundary condition. Initially, both a and h concentrations are null over all domain compatible with BC. We integrate numerically the Eqs. (1) for two different situations which differ in degradation parameter values. The simulations run for a long period of time (5,000 steps) after which the resulting concentration a and h are stationary. Then, these concentrations will be used as input signals acting over the network in several different conditions.

The aim of the paper is to study the effects of geometrical constraints on the patterning in developmental motivated models rather than to modeling a particular system. For this reason it is not necessary to fit the parameters to reproduce experimental observation. However, as the particular model chosen for our purpose has 52 parameters, we need to establish some guidelines so as to reach stable stationary patterns before implementing massive computation. In this model, the gene expression rates involve Hill functions whose coefficients $n_{i,j}$ range from 1 to 5. $n_{i,j} > 1$ reflects the fact that *cis*-regulatory systems have usually

many binding sites for each *trans*-regulatory element. These parameters can influence the shape patterns, in particular by controlling the sharpness of the patterns. The $\theta_{i,j}$ parameters represent the threshold for switching on or off the transcription processes. They were setted in the interval [0.0,1.2]. Some patterns are very sensitive to these parameters while others are robust. In particular, the thresholds corresponding to the activation of U2, U3, and U4 by U1 are sorted in decreasing order so as to form a sequence of activation; we setted them to $\theta_{41} = 0.4$, $\theta_{31} = 0.6$ and θ_{21} ranges from 0.9 to 1.2. The diffusion constants and degradation rates are initially the same for all biochemical species (0.01 and 0.20 respectively). Initially, the level of noise was null for all species. Table 1 and 2, display the parameters values used for most computations, otherwise we will mention other parameters values.

The set of partial differential equations were discretized using standard finite difference methods. The resulting large-scale dynamical system was integrated in time using forward Euler integration. We have performed simulations for different sets of parameters subject to the above mentioned restrictions. We have found that patterns are sensitive to the spatial profile concentration of a and h and the parameters that regulate the activation and repression of U1 expression, θ_{1a} , θ_{1h} and θ_{11} . For any given profiles a and h , there are regions in the parameters space where no patterns form, mainly due to the fact that activator concentration a does not reach the threshold θ_{1a} . An interplay of these parameters and both a and h profiles control the position and the coarse-grain aspect of the pattern shapes.

Figure 4 depicts the density of concentrations of u_2 (A), u_3 (B), u_4 (C) and u_5 (D) obtained using the input profile 1 (see Table 1) after 400 time steps, when stationarity is reached. We can see that the concentrations present complementary aspects. In general, the pattern of the output level is particularly complex as it is under the effects of four regulatory fields. In contrast, the concentration corresponding to u_2 is the simplest one because the regulatory field is almost homogenous in its expression domain. We have observed trough several simulations that these characteristics are quite general.

The remarkable observation in our study is the fact that geometrical constraints play a key role when surrounding tissues secret morphogenic substances. Localized patterns, similar to those developed in the semi-elliptic domain, were not formed in a semi-circular domain. In the last case, we were not able to tune the parameters in order to obtain patterns different from semi-circular stripes as shown in Figure 5. The reason for that is based on the fact that

(despite of diffusively substance a and h are uniformly secreted by the surrounding tissue) the curvature of the tissues is not homogenous in the elliptic case, but it is homogenous in the circular case. The two fronts of secreted substances are able to generate a localized expression domain for U1 in the non-homogenous curvature case. The position where the complex structures develop in Figure 4 corresponds to the maximal value of the surrounding tissue curvature. In contrast, for homogenous curvature the expression domains are not localized and that does not depend on tuning adequately the network parameters.

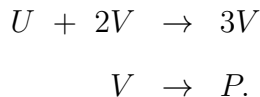
The same network can generate different patterns depending on the parameters values and the input profiles. Fig. 6 illustrates four patterns of expression level corresponding to u_5 after 400 steps. The patterns displayed at the top (A and B panels) have been obtained using profiles 1 (see Table 1) and two different sets of parameter values. In panel A the system reached stationarity, while panel B reached stationarity after 800 steps (see Movie 1). Stationary patterns displayed at the bottom (C and D panels) have been obtained using profiles 2 (see Table 1). The parameter values are shown in Table 3. Often different sets of parameter values lead to the same expression pattern, but the way to reach this pattern can differ from set to set. The movie 1 illustrates the evolution of the network in two different conditions. The right panel of the movie corresponds to the same condition as in Fig. 6B, while in the left panel we changed slightly the value of parameter to $r_3 = 32.1 \times 10^{-2}$. Both simulations correspond to 800 steps. We can see that the final patterns are almost the same, but their evolutions are quite different. Small perturbations of boundary conditions affect the patterning processes differently, depending on the network parameters. For example, Fig. 7 shows patterns generated by the network in the same conditions as in Fig. 6, but with a perturbation in the boundary tissues (both in C and C'). The panels of Fig. 7 illustrate that the perturbation can affect a little, as in panel A, or too much, destroying completely the patterns as in panels C and D. This result suggests that the shape of the tissue strongly influences the formation of pattern expression and biochemical interactions are not a necessary condition to explain alterations in the resulting gene expression patterns. The influence could be through the geometrical constraint imposed by the surrounding tissues.

In general, genetic network which underlie the developmental programs of living cells, must withstand considerable random perturbations. This occurs as fluctuation in, for example, transcription, translation, and RNA and protein degradation [33, 34]. We have also studied by numerical simulation the effects of the noise on the patterns in two situations. For

all the previous cases we have setted $r_{22} = 0.0$, i.e. there is no autocatalytic feedback acting over u_2 . It would be interesting to compare the effect of noise when this positive feedback loop is present in the network. Figures 8 and 9 show the expression profiles of u_3 and u_5 respectively, obtained for five different levels of noise $\eta = 0.00$ (A and F), $\eta = 0.05$ (B and G), $\eta = 0.10$ (C and H), $\eta = 0.15$ (D and I) and $\eta = 20$ (E and J). In both figures the top panels (A-E) correspond to the network without the above mentioned autocatalytic loop, while the bottom panels correspond to the network with the loop. The network parameter values used in both cases were the same as those used in Figure 7A, except for parameters r_{21} and r_{22} , which in the case of the network with the loop, change from 6.85×10^{-2} to 4.84×10^{-2} , and from zero to 4×10^{-2} respectively. We can see that pattern structure remains almost unaltered for noise level smaller than $\sim 10\%$ for the network with the autocatalytic loop. On the other hand, when this loop is absent ($r_{22} = 0.0$), the patterns seem to be more noise sensitive. This example illustrate that the network is robust against a considerably high level of noise. This robustness could arise from the fact that there are two negative loops underlying the regulatory interactions. Furthermore, this example shows, as in many homeotic genes, that the positive feedback loop helps the maintenance of their expression, thus contributing to the stabilization of the patterns.

B. Geometrical constraints and self-organized strategy

In order to study the influence of geometrical constraints on a self-organized system type, we have also implemented the Gray-Scott model on the semi-circular and semi-elliptical domains. The Gray-Scott model is a variant of the autocatalytic Selkov model of glycolysis which corresponds to the following two irreversible reactions:



P is an inert product. Both U and V are removed by the feeding process. A variety of spatio-temporal patterns were derived in response to finite-amplitude perturbation [35]. We consider that u and v are coupled to the activator field a and an to inhibitor h as follows:

$$\begin{aligned} \dot{u} &= D_u \nabla^2 u - uv^2 + F(1 - u) + r_u f(a, h) \\ \dot{v} &= D_v \nabla^2 v + uv^2 - (F + k)v + r_v g(a, h), \end{aligned} \tag{8}$$

where

$$f(a, h) = s^+(a, \theta_{u,a}, n_{u,a}) s^-(h, \theta_{u,h}, n_{u,h})$$

$$g(a, h) = s^+(a, \theta_{v,a}, n_{v,a}) s^-(h, \theta_{v,h}, n_{v,h}).$$

We study numerically the response to different positioned perturbations of the system which evolve in both geometries mentioned above. The initial condition corresponds to the trivial state ($u = 1$ and $v = 0$). A 16 by 16 mesh point area located over the semimajor (horizontal) axis was perturbed to $u = 0.50$ and $v = 0.25$. The system suffers the influence of a and h fields determined by the profile 1 (see Table 1). Figure 10 shows the patterns obtained from the system described by Eqs. (8) on the elliptic geometry (for system response on the circular geometry see Fig. 11). The horizontal position of perturbations were centered at 38.3, 42.3, 46.3, 50.3 and 54.3; while parameter k ranges from 0.060 to 0.066 and is uniformly spaced. Other adopted parameters are shown in Table 4. As we can see, for the several values of the parameter k , the final patterns upon 2,000 time steps depend strongly on the position where the perturbation occurs; while the geometry of the domain, either elliptical or circular, seems to have very little influence. It should be mentioned that, in contrast to the patterns derived in the previous section, these patterns are not stable, they continue growing until all the domain is filled.

IV. DISCUSSION

Early development of multicellular organisms is marked by a rapid initial increase in their cell numbers, accompanied by morphogenetic processes leading to the gradual formation of organs of characteristic shapes. During morphogenesis, through differentiation under strict genetic control, cells become more and more specialized. Further, genetic mechanisms as morphogenesis also require generic physical principles, such as, diffusion, spreading, differential adhesion, chemotaxis, etc.. As a consequence, development rely on an intricate interplay of generic and genetic mechanisms. In this paper, we have addressed the issue on how chemical signaling derived from surrounding tissues can drive patterning processes. Our results, derived by computer simulation, suggest that the shape of the source (tissue) and other geometrical constraints strongly influence the formation of complex structures. In particular, we found that non-homogenous curvature of signaling tissues can generate

complex patterns when acting on gene network, while the same network embedded in a geometry with homogenous curvature (boxes and circles) does not form localized structures. This result suggests an important consequence for development: let us consider that the shape of an organizer (tissue I or II in our case) is controlled by a gene network A, and the genic response to the organization field is controlled by a network B (the network shown in Fig. 3 in our case), which is not regulated by genes of network A. Any mutation in A that alters the shape of the organizer and consequently the organization field, will affect the development of the induced structure or organ. Thus, we can conclude that biochemical interaction is not a necessary condition to explain alteration in the overall induced output; the interaction could be underlaid by a geometrical constraint imposed by the organizer. In contrast to this hard-wire system, the self-organized system examined here (Gray-Scott model) seems to be more insensitive to the gradients derived from surrounding tissues.

We have also studied the robustness of patterns in response to noise. In this sense, two kinds of network have been used to illustrate the effect of noise in either the presence or absence of a positive feedback loop. The pattern driven by the first network seems to present higher robustness to noise than the second one. However, the two negative feedback loops presented in both cases were able to guarantee the stability of the pattern structure against a considerably high level of noise.

Although we have used a particular network topology with several mutually-inhibiting factors, there are many other possibilities for the topology that could produce interesting patterns. Each topology can response in a different way to the intrinsic noise of the patterning process. The particular case examined here was enough to conclude that the hard wired mechanism, as the regulatory networks can create complex biological shapes out of a simple structure. This mechanism could be enriched by incorporating geometrical constraint as key ingredients of morphogenesis processes.

Acknowledgments

Luciano da F. Costa is grateful to FAPESP (process 99/12765-2), CNPq (process 308231/03-1) and Human Frontier (RGP 39/2002) for financial support. Luis Diambra

thanks Human Frontier for his post-doc grant.

- [1] C.D. Doe and C.S. Goodman. *Dev. Biol.* **111**, 206 (1985).
- [2] K. Sander and P.E. Faessler. *Int. J. Dev. Biol.* **45**, 1 (2001).
- [3] T. Adachi-Yamada and M.B. O'Connor. *Dev. Biol.* **251**, 74 (2002).
- [4] L.A. Moore, H.T. Broihier, M. Van Doren, L.B. Lunsford and R. Lehmann. *Development* **125**, 667 (1998).
- [5] J.B. Gurdon, P.-Y. Bourillot. *Nature* **413**, 797 (2001).
- [6] J.B. Gurdon, S. Dyson and D. St. Johnston. *Cell* **95**, 159 (1998).
- [7] P.A. Wilson and A. Hemmati-Brivanlou. *Nature* **376** 331 (1995).
- [8] M. Strigni and S.M. Cohen. *Semin. Cell. Dev. Biol.* **10**, 335 (1999).
- [9] A.J. Koch and H. Meinhardt. *Rev. Mod. Phys.* **66** 1481 (1994).
- [10] A.M. Turing. *Philos. Trans. R. Soc. London* **237**, 37 (1952).
- [11] K.J. Painter, P.K. Maini and H.G. Othmer. *Proc. Natl. Acad. Sci. USA* **96**, 5549 (1999).
- [12] D.E. Clyde, M.S.G. Corado, X. Wu, A. Paré A, D. Papatsenko and S. Small. *Nature* **426**, 849 (2003).
- [13] P.W. Ingham. *Nature* **335**, 25 (1988).
- [14] Y. Saga and H. Takeda. *Nature Reviews* **2** 835 (2001).
- [15] A. Gossler and M. Hrabe de Angelis. *Curr. Top. Dev. Biol.* **38**, 225 (1998).
- [16] N.A.M Monk. *Endeavour* **24**, 170 (2000).
- [17] L. Wolpert, R. Beddington, T. Jessel, P. Lawrence, E. Meyerowitz and J. Smith. *Principles of Development*, Oxford: Oxford University Press.
- [18] M. Freeman. *Nature* **408** 313 (2000).
- [19] I. Salazar-Ciudad and J. Jernvall. *Proc. Natl. Acad. Sci. USA* **99**, 8116 (2002).
- [20] S.Y. Shvartsman, C.B. Muratov and D.A. Lauffenburger. *Development* **129**, 2577 (2002).
- [21] G. von Dassow, E. Meir, E.M. Munro, G.M. Odell. *Nature* **406**, 188 (2000).
- [22] R.A. Barrio, C. Varea, J.L. Aragon and A Maini, *Bull. Math. Biol.* **61**, 483 (1999).
- [23] R. Plaza, F. Sanchez-Garduno, P. Padilla, R.A. Barrio and P.K. Maini, *J. Dyn. and Diff. Eq.* **16**, 1093 (2004).
- [24] A.A. Teleman, M. Strigini, and M.S. Cohen, *Cell* **105**, 559 (2001).

- [25] N. McDowell, J.B. Gurdon and D.J. Grainger. *Int. J. Dev. Biol.* **45**, 199 (2001).
- [26] E.V. Entchev, A. Schwabedissen, M. Gonzalez-Gaitan. *Cell* **103**, 981 (2000).
- [27] F.A. Ramirez-Weber and T.B. Kornberg. *Cell* **97**, 599 (1999).
- [28] V. Greco, M. Hannus and S. Eaton. *Cell* **106**, 633 (2001).
- [29] J. Dubrulle, M.J. McGrew and O. Pourquie. *Cell* **106**, 219 (2001).
- [30] J. Reinitz and D.H. Sharp. *Mech. Dev.* **49**, 133 (1995).
- [31] P. Smolen, P.E. Hardin, B.S. Lo, D.A. Baxter and J.H. Byrne. *Biophys. J.* **86**, 2786 (2004).
- [32] T. Mestl, E. Plahte and S.W. Omholt. *J. Theor. Biol.* **176**, 291 (1995).
- [33] A. Arkin, J. Ross and H.H. McAdams. *Genetics* **149**, 1633 (1998).
- [34] H.H. McAdams and A. Arkin. *Proc. Natl. Acad. Sci. USA* **94**, 814 (1997).
- [35] J.E. Pearson. *Science* **261**, 189 (1993).

Tables

TABLE I: Parameter values for diffusion, degradation and geometrical constraints used to obtain the input profiles 1 and 2. These profiles differ in the degradation values γ_a and γ_h which were reduced to 0.5×10^{-3} to generate the input profile 2.

Parameters	Values	Parameters	Values
d_i	0.01	<u>Semi-ellipse</u>	
γ_i ($i \neq 5$)	0.20	internal semimajor axis	40.00
γ_5	0.35	internal semiminor axis	14.14
D_a	0.04	external semimajor axis	86.60
D_h	0.04	external semiminor axis	31.62
γ_a	1.0×10^{-3}	<u>Semi-circular</u>	
γ_h	1.0×10^{-3}	internal radius	24.70
Δt	1.00	external radius	51.96
Δx	0.40		

TABLE II: Parameter values of the gene network used to obtain the pattern shown in Figure 4. These values were also used in other simulations whenever we have not stated otherwise (see also Table III).

Parameters	Values	Parameters	Values
r_1	6.25	r_4	5.8×10^{-2}
θ_{1a}	0.40	θ_{41}	0.40
θ_{1h}	0.05	θ_{42}	0.25
θ_{11}	0.20	θ_{43}	0.20
n_{1a}	1.00	n_{41}	4.00
n_{1h}	3.00	n_{42}	2.00
n_{11}	5.00	n_{43}	2.00
r_{21}	8.06×10^{-2}	r_5	20/27
θ_{21}	1.05	θ_{51}	0.55
θ_{23}	0.35	θ_{52}	0.20
θ_{24}	0.45	θ_{53}	0.30
n_{21}	4.00	θ_{54}	0.50
n_{23}	2.00	n_{51}	4.00
n_{24}	2.00	n_{52}	3.00
r_3	0.21	n_{53}	3.00
θ_{31}	0.60	n_{54}	3.00
θ_{32}	0.10	PFL parameters	
θ_{34}	0.10	r_{22}	0.00
n_{31}	4.00	θ_{22}	0.10
n_{32}	2.00	n_{22}	3.00
n_{34}	2.00		

TABLE III: Parameter values of the gene network used to obtain the patterns shown in Figure 7. The values of parameters not shown in this table are the same as in Table II.

Fig. 7A		Fig. 7B		Fig. 7C		Fig. 7D	
Parameters	Values	Parameters	Values	Parameters	Values	Parameters	Values
r_{21}	6.85×10^{-2}	r_1	9.25	r_1	7.50	r_1	7.50×10^{-6}
θ_{21}	0.99	θ_{11}	0.265	θ_{1a}	0.20	r_{21}	8.46×10^{-2}
n_{21}	5.00	r_{21}	12.09×10^{-2}	r_{21}	12.09×10^{-2}	θ_{21}	0.95
r_3	0.215	θ_{21}	0.85	θ_{21}	1.30	n_{21}	5.00
θ_{31}	0.65	n_{21}	5.00	n_{21}	5.00	r_3	0.27
r_4	5.60×10^{-2}	r_3	32.02×10^{-2}	r_3	0.18	n_{31}	2.00
r_5	0.18	r_4	6.24×10^{-2}	r_4	5.20×10^{-2}	r_4	9.75×10^{-2}
θ_{51}	0.50	r_5	35/216	r_5	10/9	θ_{41}	0.45
θ_{52}	0.55	θ_{51}	0.50	θ_{51}	0.52	θ_{42}	0.20
θ_{53}	0.50	θ_{52}	0.40	θ_{52}	0.40	n_{41}	2.00
θ_{54}	0.20	n_{51}	2.00	θ_{53}	0.30	r_5	8.54
n_{51}	2.00			θ_{54}	0.25	θ_{51}	0.50
				n_{51}	3.00	θ_{52}	0.40
						θ_{53}	0.20
						θ_{54}	0.20
						n_{51}	2.00

TABLE IV: Parameter values for the Gray-Scott model.

Parameters	Values	Parameters	Values
F	0.04	$\theta_{ua}(= \theta_{uh})$	0.50
r_u	0.001	$\theta_{va} = \theta_{vh})$	0.50
r_v	0.002	$n_{ua}(= n_{uh})$	1.0
D_u	0.0336	$n_{va}(= n_{vh})$	1.0
D_v	0.0168		

Figures and movie

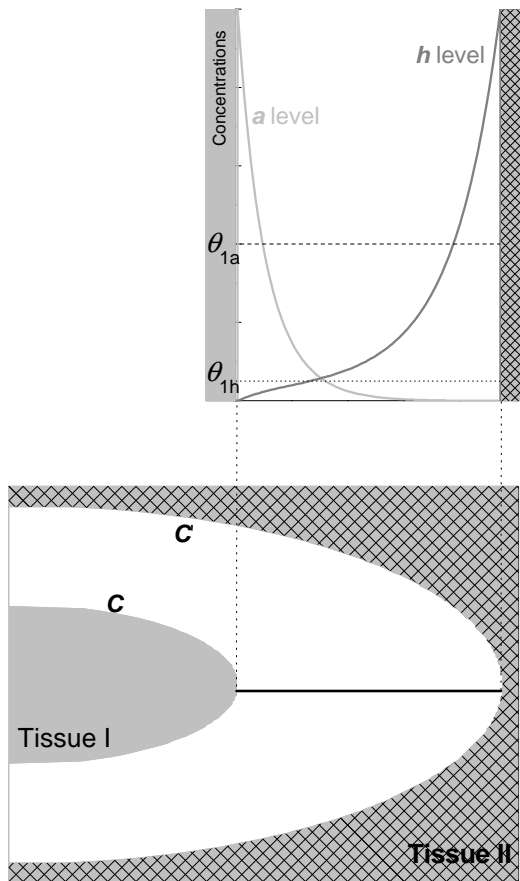


FIG. 1: A schematic representation of surrounding tissues, boundaries (bottom) and the concentration profile of activator a and inhibitor h over a horizontal segment in the middle of a semi-elliptic domain (top).

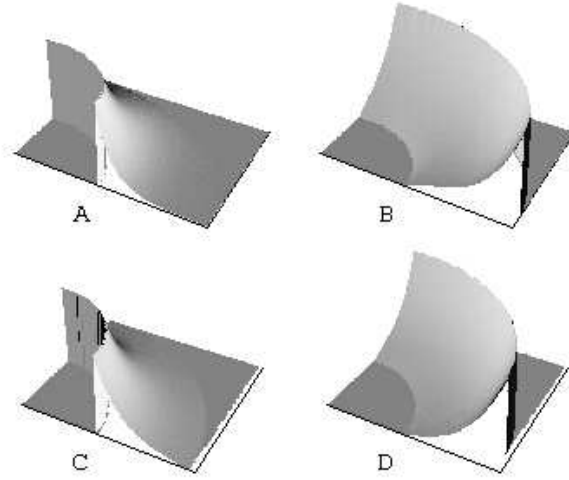


FIG. 2: 3D plots of the concentration of a , secreted by the tissue I (A and C), and h (B and D) which is secreted by the tissue II, obtained from Eqs. 1, after 5,000 time steps. The panels A and B correspond to the elliptical geometry, and panels C and D correspond to the circular geometry.

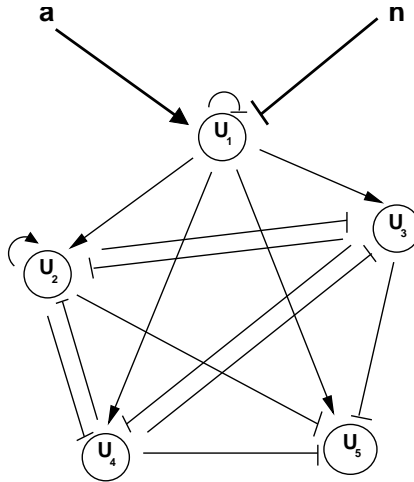


FIG. 3: Schematic diagram of the network. Circles indicate genes, blunt-end arrows denote inhibition and pointed arrows denote activation. Regulatory activation is represented by arrows and regulatory inhibition by small perpendicular edges, as usually. This network presents two negative feedback loops, one where U_2 inhibits U_3 that inhibits U_4 that inhibits U_2 ; and another which is formed by U_4 that inhibits U_3 that inhibits U_2 that inhibits U_4 . There is also an auto-inhibitory loop acting over U_1 and an autocatalytic loop acting over U_2 .

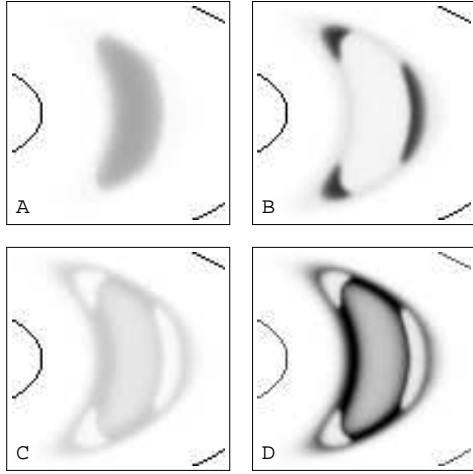


FIG. 4: Density plot of concentrations of u_2 (A), u_3 (B), u_4 (C) and u_5 (D) after 400 steps in a semi-elliptic domain. The model parameters used to compute these patterns are displayed in Table.

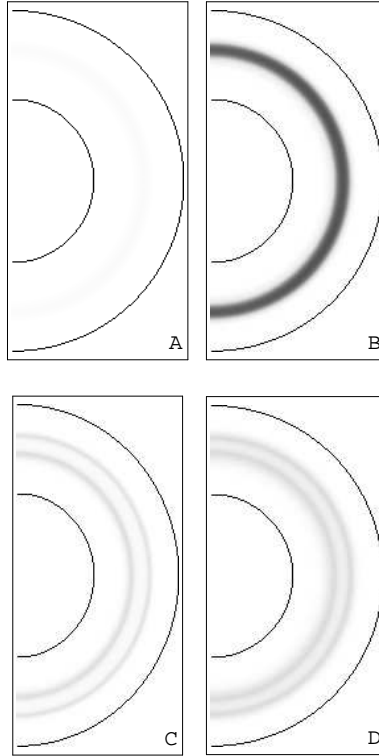


FIG. 5: Density plot of concentrations of u_2 (A), u_3 (B), u_4 (C) and u_5 (D) after 400 time steps. In this semi-circular domain, no localized structure were observed for any set of parameter values.

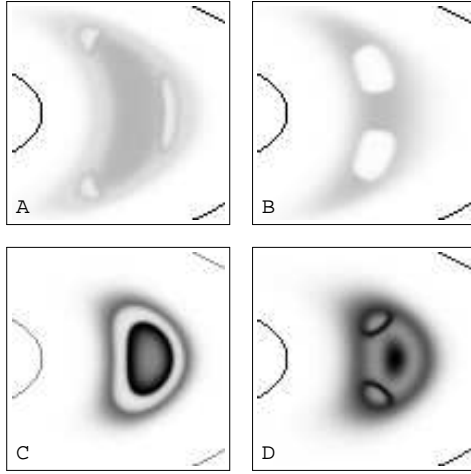


FIG. 6: Density plot of concentrations of u_5 after 400 obtained for inputs profile 1 (A and B) and inputs profile 2(C and D) with the network parameters displayed in Table 3.

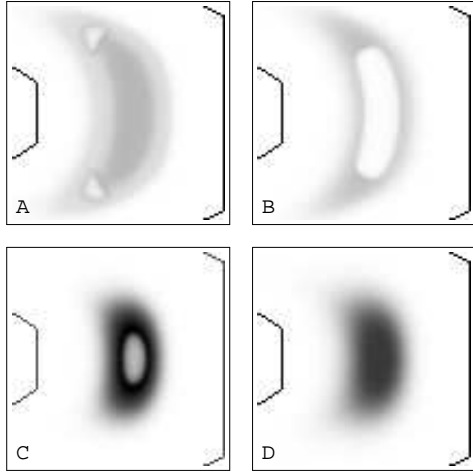


FIG. 7: Density plot of concentrations of u_5 after 400 steps obtained in the same condition that Fig. 6 with the exception in the boundary condition which were perturbed.

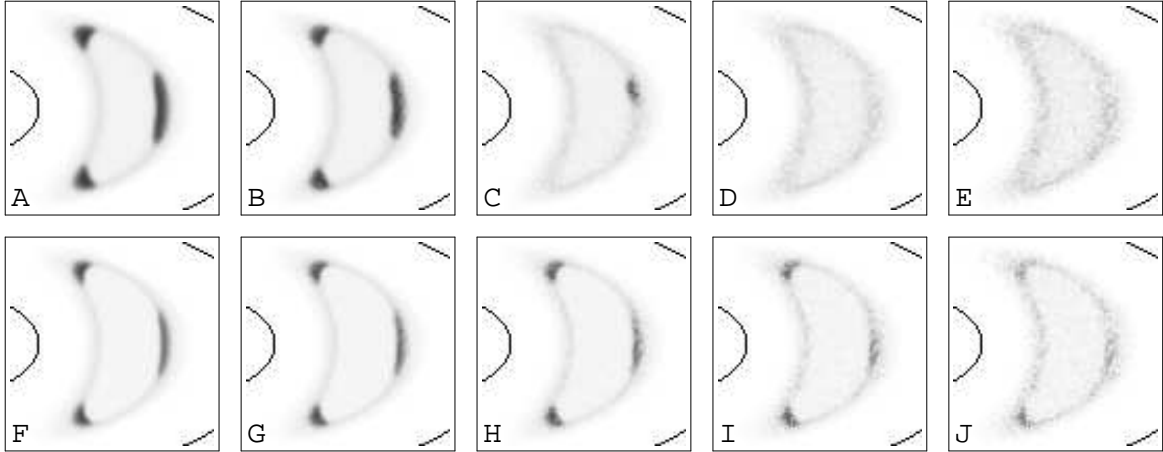


FIG. 8: Density plot of u_3 obtained, after 400 steps, when the dynamics of the gene network is perturbed with noise. The top panels correspond to patterns obtained from the network without the positive feedback loop for increasing level of noise (sorted from left to right). The bottom panels correspond to patterns obtained from the network with the feedback loop for increasing level of noise (sorted from left to right). The level of noise used were $\eta = 0.0$ (A and F) $\eta = 0.05$ (B and G), $\eta = 0.10$ (C and H), $\eta = 0.15$ (D and I), and $\eta = 0.20$ (E and J). For further information, see the text.

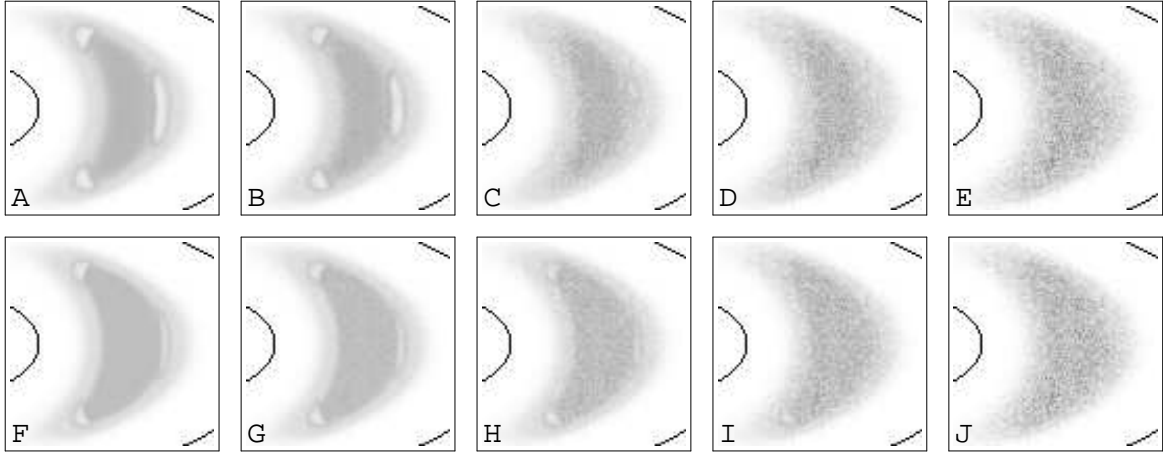


FIG. 9: Density plot corresponding to u_5 obtained in the same situation as in Fig. 8.

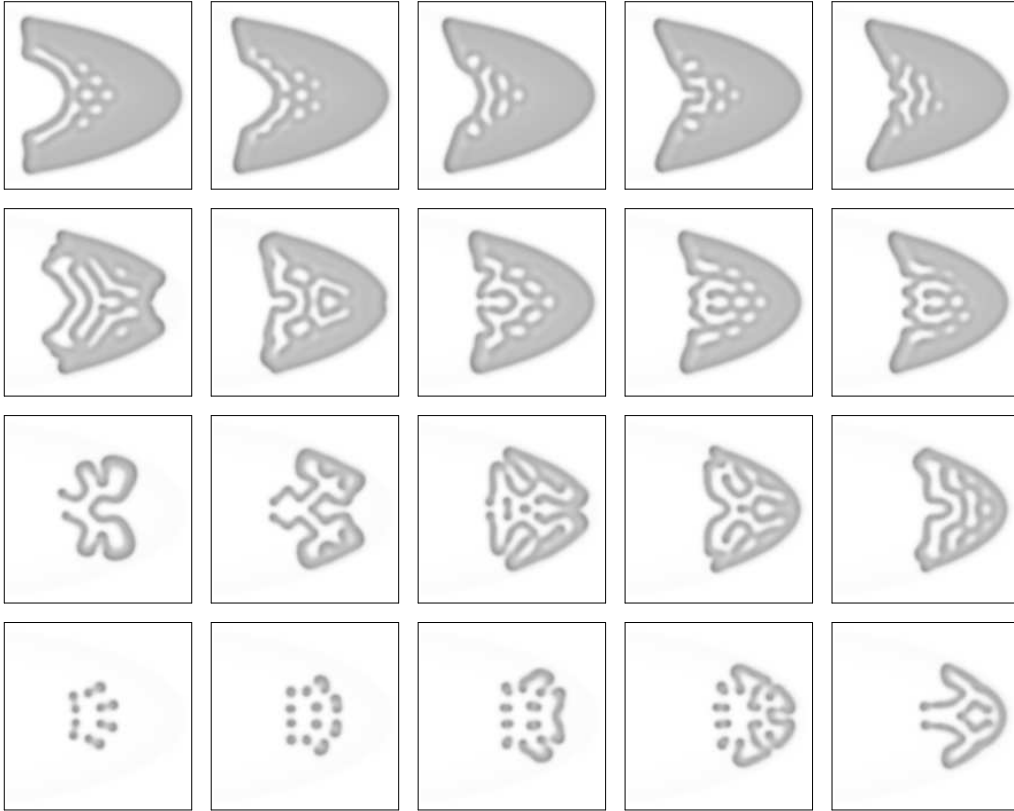
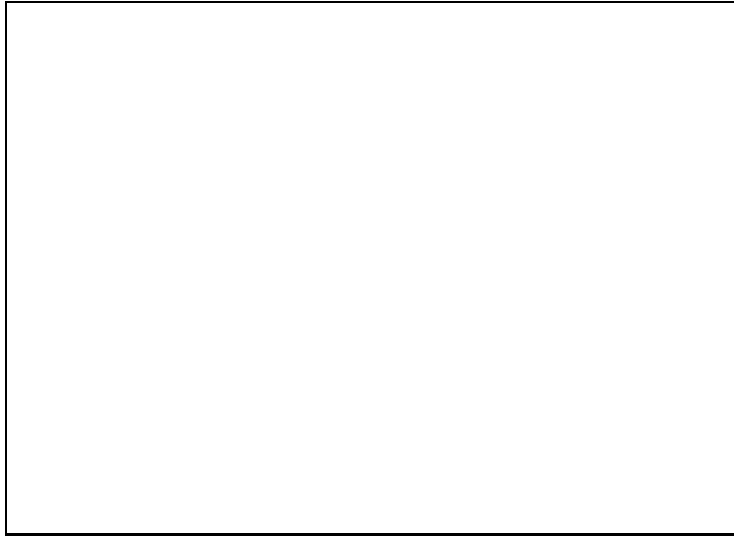


FIG. 10: Elliptic Geometry: Density plot of the v concentration for different position of perturbation, increasing from left to right, and for different values of parameter k which increases from top to bottom (see details in text).



FIG. 11: Circular Geometry: Density plot of the v concentration for different positions of perturbation (increasing from left to right) and for different values of parameter k (increasing from top to bottom).



Movie 1: (Please see at <http://glia.if.sc.usp.br/luis/teste.mov>) The left panel corresponds to the temporal evolution of the pattern Fig. 7B during 800 steps. The right panel corresponds to the evolution in the same condition with the exception of pattern r_3 which changes from 32.02×10^{-2} to 32.1×10^{-2}